ACS APPLIED MATERIALS & INTERFACES

Research Article

www.acsami.org

Fast and Selective Room-Temperature Ammonia Sensors Using Silver Nanocrystal-Functionalized Carbon Nanotubes

Shumao Cui,[†] Haihui Pu,[†] Ganhua Lu,[†] Zhenhai Wen,[†] Eric C. Mattson,[‡] Carol Hirschmugl,[‡] Marija Gajdardziska-Josifovska,[‡] Michael Weinert,[‡] and Junhong Chen*[,†]

[†]Department of Mechanical Engineering and [‡]Department of Physics and Laboratory for Surface Studies, University of Wisconsin–Milwaukee, Milwaukee, Wisconsin 53211, United States

Supporting Information

ABSTRACT: We report a selective, room-temperature NH_3 gas-sensing platform with enhanced sensitivity, superfast response and recovery, and good stability, using Ag nanocrystal-functionalized multiwalled carbon nanotubes (Ag NC–MWCNTs). Ag NCs were synthesized by a simple mini-arc plasma method and directly assembled on MWCNTs using an electrostatic force-directed assembly process. The nanotubes were assembled onto gold electrodes with both ends in Ohmic contact. The addition of Ag NCs on MWCNTs resulted in dramatically improved sensitivity toward NH_3. Upon exposure to 1% NH_3 at room temperature, Ag NC–MWCNTs showed enhanced sensitivity (~9%), very fast response (~7 s), and full recovery within several minutes in air. Through density functional theory calculations, we found that the fully oxidized Ag surface plays a critical role in the sensor response. Ammonia molecules are adsorbed at Ag hollow sites on the AgO surface with H pointing toward Ag. A net charge transfer from NH_3 to the Ag NC–MWCNTs hybrid leads to the conductance change in the hybrid.

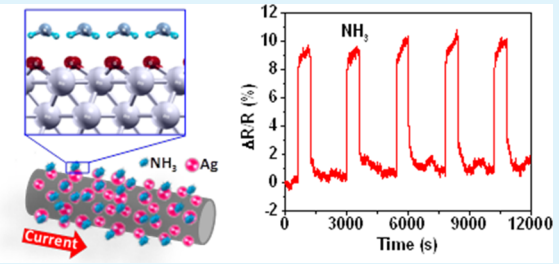

KEYWORDS: *ammonia gas sensor, nanohybrid, silver nanocrystal, carbon nanotube, high performance, room-temperature*

INTRODUCTION

A gas sensor is a device that can detect gas information (composition, concentration) of a local environment. It is critical in many fields of our life, including environmental monitoring, industrial process control, clean energy deployment, and medical diagnosis. Research on sensing materials primarily focuses on enhancing sensitivity, selectivity, stability and response/recovery time. A low operation temperature is also a necessity for specific flammable gases such as H_2 and important for lower power consumption. Nanostructured sensing materials, such as nanowires, nanotubes, and nanoparticles, are promising because of their high surface-to-volume ratio, small size, low energy consumption, and unique electronic properties.[1−4]

Carbon nanotubes (CNTs) have attracted extensive interest in various applications since their discovery in 1991, because of their extraordinary mechanical, electrical, and chemical properties.[5−9] In 2000, Kong et al. showed that single-walled carbon nanotubes (SWCNTs) exhibit high sensitivity to NO_2 and NH_3 at room temperature,[10] which inspired researchers to widely explore CNTs for room-temperature gas sensors. Generally, the gas-sensing mechanism of CNTs is based on the resistance change due to the charge transfer between adsorbed gas molecules and CNTs. Oxidizing gases (e.g., NO_2) withdraw electrons from CNTs, whereas reducing gases (e.g., NH_3) donate electrons, which could lead to significant changes in the electrical resistance of CNTs.

Pristine CNTs have strong sp^2 carbon–carbon bonds, making them chemically stable and difficult to form strong bonding with most gas molecules. Theoretical calculations have been carried out to understand the adsorption of various gases on CNTs, including NH_3, NO_2 and H_2, and the results showed that most of the molecules are weakly adsorbed on the surface of CNTs.[11] Therefore, bare multiwalled CNTs (MWCNTs) exhibit limited sensing performance (low sensitivity, relatively long response and recovery time, and poor selectivity) to some gases, such as NO_2 and NH_3,[12,13] and insensitivity to other gases such as H_2 and CO, according to previous experimental studies.[14] The limited sensitivity can be explained by the known defects and adsorbed oxygen on the sidewall of CNTs.[9,10,15] However, CNTs-based gas sensors with improved sensitivity and selectivity can be obtained by functionalizing CNTs sidewalls with specific materials. Noble metals have been widely used to increase the sensitivity and selectivity of gas sensors. For example, Pd was generally used to functionalize CNTs for hydrogen sensing because of its high hydrogen solubility.[14,16] Various other metals also have been studied and have showed enhancement in gas sensing applications.[13,17] Although Ag nanocrystals (NCs) have rarely been studied as functional additives on CNTs to enhance the sensing performance, Ag mesowire arrays have been reported for a fast reversible NH_3

Received: July 4, 2012
Accepted: August 9, 2012
Published: August 9, 2012

sensor with high sensitivity.[18] However, the sensor fabrication is complex and lacks control over the electrodeposition of Ag on highly oriented pyrolytic graphite, causing a wide variation in sensitivity for similar Ag mesowire arrays. In addition, Ag mesowires-based sensors are only sensitive to ammonia at concentrations above 1%.

Ammonia is commonly produced from the waste product of livestock or from industry and automobile emissions.[19] It is an environmental concern because of serious health threat with exposure to high concentrations of NH_3.[20] For example, short time exposure to high ammonia concentrations, 0.1% or more, can cause severe long-term respiratory system disorder; exposure to ammonia of extremely high concentrations, 0.5%−1%, is suggested to be lethal within 5−10 min. Therefore, it is critical to develop fast and selective ammonia sensors toward these high ammonia concentrations. Here we report on fast and selective NH_3 sensing properties of Ag NC−MWCNT hybrid structures at room temperature. We found that Ag NCs significantly enhanced the sensitivity, response, and recovery of CNT sensors. Furthermore, the Ag NC−MWCNT sensor had good stability and selectivity, with detection concentrations varying from 0.125% to 1%. Density functional theory (DFT) calculations were carried out to reveal the interaction between NH_3 and Ag.

EXPERIMENTAL SECTION

Sensor Fabrication and Structural Characterization. Sensors were fabricated using a similar process as we reported before.[3,21] Interdigitated gold electrodes with finger width and inter-finger spacing of 2 μm and a thickness of 50 nm were fabricated using e-beam lithography on a silicon substrate with a SiO_2 thin top layer. To bridge the gold electrodes with MWCNTs, MWCNTs (20−30 nm in diameter) were first uniformly dispersed in N, N-Dimethylformamide (DMF) by ultrasonication. Then a tiny drop (1 μl) of MWCNTs solution was drop cast on the gold electrodes. After DMF evaporated, MWCNTs were left, connecting the gold fingers. The amount of MWCNTs on gold electrodes can be controlled by adjusting the dispersion concentration. In this study, we used a very low CNT concentration, and only a few MWCNTs were found bridging the gold electrode fingers after DMF drying. Further annealing treatment at 200 °C for 1 h in Ar flow (1 lpm) was carried out to remove the residual DMF and to improve the contact between MWCNTs and gold electrodes.

To synthesize Ag NC−MWCNT hybrid structures, we produced Ag NCs by physical vapor deposition using a mini-arc plasma reactor.[22] The mini-arc plasma was generated between two carbon electrodes, and small pieces of Ag (purity: 99.999%) cut from an Ag wire were used as the precursor material. After Ag was evaporated into vapor by the mini-arc plasma source, the Ag vapor was carried by an Ar flow (3 lpm) downstream and quenched through natural cooling in the copper tubing to form Ag NCs in the gas phase. The as-produced Ag NCs were directly deposited onto MWCNTs on gold electrodes using an electrostatic force directed assembly (ESFDA) process.[23] After deposition, the Ag NC−MWCNTs hybrid sensor was annealed at 200 °C for 1 h in Ar flow (1 lpm) to improve the contact between Ag NCs and MWCNTs.

The morphology and crystal structure of the Ag NC−MWCNTs hybrid were studied with a field emission scanning electron microscope (SEM) (Hitachi S4800) and a high-resolution transmission electron microscope (HRTEM) (Hitachi H-9000-NAR) with 0.18 nm point and 0.11 nm lattice resolution when operated at an accelerating voltage of 300 kV.

Ammonia Sensing Measurements. A sensor was placed into an air-tight sensing test chamber with electrical feedthroughs. A constant dc voltage was applied to the electrodes bridged by Ag NC−MWCNTs hybrids. Ammonia was detected by monitoring and recording the change of electrical current passing through MWCNTs using a Keithley 2602 source meter (Keithley, Cleveland, OH). One typical sensing test cycle has three continuous sequential steps: First, a clean dry air flow (2 lpm) was introduced into the sensing chamber as a background. Then, a test gas of NH_3 diluted in air was injected into the chamber with the same flow rate (2 lpm) to register a sensing signal. Finally, a clean dry air flow (2 lpm) was introduced again for sensor recovery. Multiple testing cycles were performed by continuously repeating the same test several times.

Density Functional Theory (DFT) Calculation. DFT calculations were performed using the full potential linearized augmented plane wave (FLAPW) method as implemented in flair.[24] The exchange correlation is treated in the formalism of generalized gradient approximation (GGA) of Perdew, Burke, and Ernzerhof (PBE).[25] The cutoff energy of the plane wave basis was 435 eV. The Ag NC was simulated using the (111) surface slab model of four layers of atoms in the $\sqrt{3} \times \sqrt{3}$ supercell with a 8 × 8 × 2 k-point grid and a sphere radius of $2.5a_B$. The sphere radii of N and H are $1.0a_B$ and $0.6a_B$, respectively. The vacuum region was kept above 12 Å. The Ag surface was oxidized as AgO, because oxygen can be dissociated and adsorbed on an Ag (111) plane at room temperature (see Figure S1 in the Supporting Information), and the oxygen ions can migrate easily, according to our calculations. The two uppermost layers of Ag and O atoms were relaxed before gas adsorption, whereas only the topmost layer of Ag and O atoms and gas molecules were allowed to fully relax during the adsorption. The force criterion for the optimization was within 0.04 eV/Å. The charge transfer analysis was based on the Hirshfeld method.[26]

RESULTS AND DISCUSSION

Figure 1a shows the scanning electron microscopy (SEM) image of a typical Ag NC−MWCNT hybrid bridging a pair of gold electrode fingers in a realistic sensor device. The two gold electrode fingers acted as source and drain electrodes during the electrical measurements, and the Ag NC−MWCNT hybrid

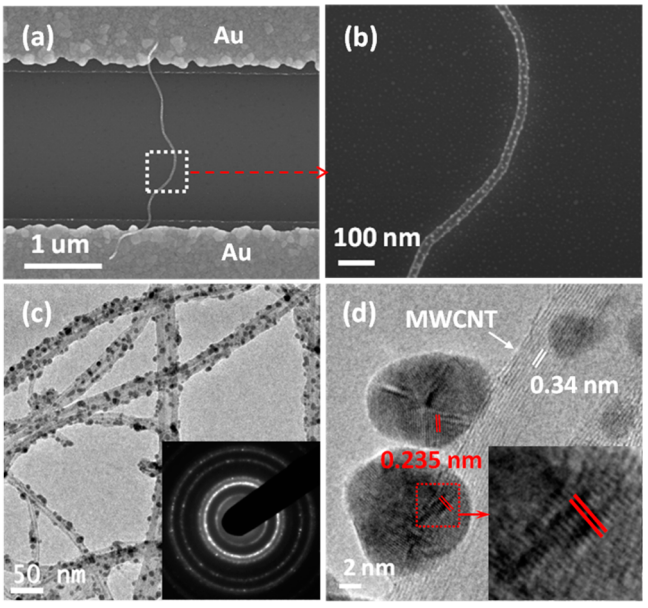

Figure 1. (a) SEM image of a representative MWCNT decorated with Ag NCs connecting two gold electrode fingers. Typically a small number of Ag NC−MWCNT hybrids bridge the gold electrode fingers in this study. (b) SEM image of the enlarged view of Ag NC−MWCNT structure as marked in a. (c) TEM image of Ag NC−MWCNT hybrid structures. The inset is an SAED pattern of the hybrid demonstrating Ag crystallinity. (d) HRTEM image of Ag NC-MWCNT hybrid nanostructure. The inset is the enlarged view of Ag structure as marked on the Ag NC.

was the conducting channel as well as the active sensing material. Since MWCNTs have relatively larger diameters than SWCNTs, the resistance of MWCNTs is low. MWCNTs typically show more metallic behavior than SWCNTs because of the decreasing energy band gap with the increasing diameter.[3,27] In this study, a small number of MWCNTs was used. Figure 1b is a close-up view of the Ag NC-MWCNT segment boxed in Figure 1a, showing the detailed morphology of the Ag NC−MWCNT hybrid structure. A transmission electron microscopy (TEM) image of the hybrid structure is shown in Figure 1c. It is evident that Ag NCs decorate MWCNTs in a noncontinuous manner, and the NCs distribution is quite uniform. The size of Ag NCs ranges from several nanometers to about 10 nm. The inset in Figure 1c shows a selected area electron diffraction (SAED) pattern of the hybrid proving that the Ag nanoparticles are crystalline. Besides the innermost ring, which belongs to MWCNTs, the other four bright rings are indexed to cubic fcc (111), (200), (220), and (311) lattice planes of Ag metal from the inside to the outside.[28] Figure 1d shows the high-resolution TEM (HRTEM) image of an individual MWCNT decorated with Ag NCs. The measured lattice spacing of 0.235 nm for the NCs corresponds to (111) plane of Ag. The smaller nanoparticles are single crystal, and the larger ones exhibit stacking faults often seen in colloidal gold and silver NCs. In addition to the rounded edges, the nanoparticles have some flat facets corresponding to the most densely packed {111} surface plane terminations.

Figure 2a shows the *I*−*V* characteristics of MWCNTs before and after Ag NCs deposition. The straight lines indicate that

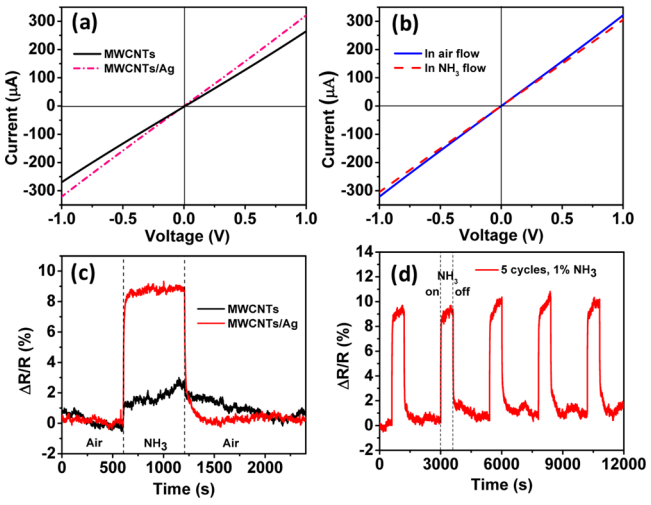

Figure 2. (a) *I*−*V* characteristics of MWCNTs before and after Ag NCs decoration. (b) *I*−*V* characteristics of Ag NC−MWCNT hybrid sensors in airflow and in 1% NH_3 flow. (c) The room temperature dynamic sensing response (ΔR/R) before and after Ag NCs decoration. (d) Five sensing cycles of the Ag NC−MWCNT hybrid sensor to 1% NH_3, indicating a good stability.

the contact between the MWCNTs and the gold electrodes are Ohmic, which is consistent with our previous report.[3] In our experiments, annealing treatment at 200 °C for 1 h in Ar flow was performed after MWCNT deposition to improve the electrical contacts. According to the literature,[29] MWCNTs show more metallic behavior than SWCNTs, and the outermost shell of MWCNT is responsible for the electrical transport. Therefore, even with a smaller contact area compared with the use of additional Pt or Au deposition to enhance the CNT−electrode contact, charge carriers can still flow smoothly between MWCNTs and gold electrodes after the annealing. Therefore, the Schottky barrier (SB) between the MWCNT and the electrodes was minimized in our sensor and the main mechanism of sensing is a direct charge transfer between the adsorbed gas molecules and the Ag NC−MWCNTs.[30] On the basis of the measurements, the resistance of bare MWCNTs is ∼3.4 kΩ, indicating typical good conductance of MWCNTs. After Ag NCs deposition on the MWCNTs and annealing in an Ar atmosphere, the resistance of MWCNTs decreased to a value of ∼3.1 kΩ. Knowing from microscopic images that Ag NCs do not form interconnected conducting pathways along MWCNTs, it is logical to attribute the decrease in resistance to a net charge transfer between the Ag NCs and MWCNTs. It is well known that Ag is a catalytic material and can dissociate and chemisorb O_2 in the presence of oxygen molecules under atmospheric conditions,[31] which is confirmed by our DFT calculations (see Figure S1 in the Supporting Information). Thus, nano-scopic electron depletion zones form around Ag NCs because of surface oxidation, which gives rise to so-called nano-Schottky barriers. The work function of these regions (5.4−5.6 eV)[32] is higher than those of MWCNTs (4.7−4.9 eV),[31] which allows a net electron transfer from MWCNTs to Ag NCs and causes a decrease in the resistance.[33]

Ammonia sensing tests were performed in an air-tight chamber at room temperature. A constant dc bias of 2 mV was applied between the source and drain electrodes, and the current passing through the Ag NC−MWCNTs was recorded. As shown in Figure 2b, the *I*−*V* characteristics of the sensor exhibit linear behavior both in the airflow and in the NH_3 flow, indicating that the Ohmic contact between the hybrid and the gold electrode is not disturbed by the gas flow. The linear *I*−*V* curve in the NH_3 flow (dashed red line) has a slightly smaller slope than that in the airflow (solid blue line), indicating that the resistance of the Ag NC−MWCNTs hybrid increased after exposure to NH_3 due to the gas molecule adsorption and a net charge transfer between gas molecules and the hybrid. Because the device current change is relatively small compared with the device current before exposure to NH_3, the slope change is also very small but can be discerned in a magnified figure (see Figure S2 in the Supporting Information). To compare the sensing performance of MWCNTs before and after Ag NCs deposition, bare MWCNTs were tested first against NH_3. Then the same sensor was tested again after being coated with Ag NCs. The dynamic response of both bare MWCNTs and Ag NC−MWCNTs hybrids to 1% NH_3 is shown in Figure 2c. The sensitivity (S) is defined as $\Delta R/R = (R_g\text{-}R)/R$, where R is the average sensor resistance in the air before test gas exposure, while R_g is the sensor resistance after exposure to a test gas. From Figure 2c, it can be seen that a maximum sensitivity of ∼2.8% is achieved for bare MWCNTs with 10 min exposure to 1% NH_3. For Ag NC−MWCNTs, however, the sensitivity is ∼9.0% with the same exposure time, and it reached ∼8.0% instantly. This sensitivity of Ag NC−MWCNTs for 1% NH_3 exceeds that of Ag mesowire arrays NH_3 sensors, which showed ∼5% response to NH_3 with >1% concentration.[18] For Ag film prepared with the same method as Ag mesowires, the sensitivity was <5%.[18] Therefore, the Ag NC−MWCNTs sensor has higher sensitivity toward NH_3 than sensors composed of either pure MWCNTs or pure Ag, and Ag NCs play a critical role in enhancing gas sensitivity.

Although here we have shown that the sensor sensitivity was enhanced through combination of Ag NCs with MWCNTs, there is still plenty of room to further improve the sensor sensitivity, such as through tuning electronic properties of CNTs (e.g., semiconducting CNTs vs. metallic CNTs) and the Ag NC coverage on the surface of CNTs. SWCNTs with excellent semiconducting properties[10] can be used to improve the sensitivity. Furthermore, graphene nanoribbons (GNRs), which can be obtained by unzipping CNTs, are excellent semiconductors with an on-off current ratio reaching about 1×10^7,[34,35] and can be a promising material to replace CNTs for promoting the sensitivity. In addition, one-dimensional (1D) metal oxides were also reported as high-sensitivity NH_3 gas sensors, such as ZnO nanowires and In_2O_3 nanotubes.[36,37] However, the operating temperature (300 °C) is relatively high for ZnO nanowires and In_2O_3-based sensors are relatively expensive. Moreover, the response time for 1D metal oxide sensors is typically on the order of minutes.

The sensing mechanism of Ag NC−MWCNTs was studied through combining experiments with DFT calculations. Previous theoretical studies showed that NH_3 interacts weakly with pristine CNTs with little charge transfer, in agreement with the low sensitivity results in this work.[11,15,30] Therefore, the Ag NCs could strengthen the NH_3 sensing performance of the hybrid structure by acting as the dominant active adsorption regions for NH_3 in our hybrid sensor. For atmospheric pressure and room-temperature operation of such a sensor, it is important to consider the effects from oxygen, especially because silver is a semiprecious metal. From our DFT calculations, oxygen molecules can be dissociated and adsorbed on a clean Ag (111) surface resulting in an AgO monolayer structure where O atoms occupy standard fcc in-plane positions, but with large inward contraction of the oxygen plane (red atoms in Figure 3). This result is consistent with a previous report.[38] An extra negative charge is taken by the oxygen because the electron negativity of oxygen is higher than that of Ag.[39] These oxygen ions lead to electron depletion regions (nano-Schottky barrier) at the Ag NC surfaces, providing more effective adsorption sites for ammonia. Since the electron affinity of silver (2.0−2.5 eV) is high, the NH_3 (electron donor) is more likely to interact with Ag atoms on the oxidized Ag surface.[39] To understand the interaction between the oxidized Ag surface and NH_3, DFT calculations were performed, and different initial orientations of NH_3 on various surface locations (e.g., NH_3 above oxygen atom with H pointing up or pointing down) were used to find out the most stable configuration of NH_3 adsorption on the AgO surface. After full relaxation, the energetically favorable adsorption result is shown in Figure 3. It can be seen that NH_3 molecules are adsorbed above the hollow sites of AgO surface with N following the position of fcc stacking of bulk Ag, and H atoms pointing to Ag atoms instead of O atoms. A net 0.0038 e charge transfer from one NH_3 molecule to Ag was obtained. It should be noted that although Hirshfeld method is qualitatively accurate, it tends to underestimate the magnitude of charge transfer.[40] Thus, the oxidation state of Ag was reduced by the charge transfer, which leads to the electronic state change and meanwhile a conductance change in the MWCNTs channel, which is called "electronic sensitization."[41] Because the MWCNT is a p-type semiconductor in atmosphere, the charge transfer from Ag into the MWCNT causes depletion of holes in MWCNTs and an increase in the electrical resistance.

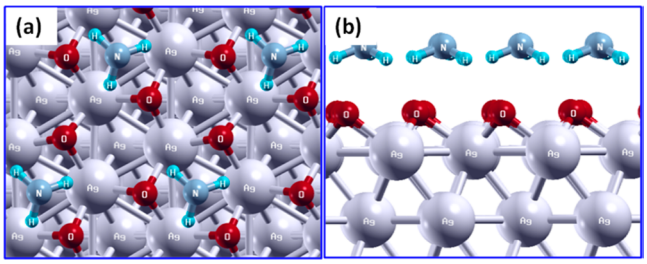

Figure 3. (a) Top and (b) side view of NH_3 adsorption on the oxidized silver (AgO) surface plane (111), with atomic positions optimized by DFT to a lowest energy configuration resulting in 0.0038 e charge transfer from NH_3 to Ag.

To further investigate the role of the oxygen coverage level on the Ag surface, we considered NH_3 adsorption on a clean Ag surface and Ag_3O surfaces in DFT calculations, and compared with the results for AgO. The results showed that NH_3 is in favor of sitting above the Ag site with binding energy of 0.40 eV on the clean Ag surface (see Figure S3 in the Supporting Information). In the case of Ag_3O, the hollow site is preferable while the binding energy increases to 0.74 eV, as opposed to the oxygen site forming a hydrogen bond with binding energy of 0.15 eV (see Figure S4 in the Supporting Information). Therefore, NH_3 is attracted to the unoxidized region at a low oxygen coverage level. The N atom is pointing to Ag in both cases, which is different from AgO where the three H atoms are pointing towards the surface. On the AgO surface, however, the NH_3 binding energy decreases to 0.36 eV in the lowest energy configuration that is shown in Figure 3. Hirshfeld charge analysis shows that NH_3 adsorbed on the clean and Ag_3O surfaces gains 0.886 e and 0.015 e, respectively, suggesting that NH_3 acts as an acceptor, contrary to what we observed in our experiment. Therefore, a fully oxidized Ag surface (AgO) is the practical case in our sensor. Actually, oxygen atoms could easily migrate on an AgO surface because of the low barrier height of 0.32 eV.

It is interesting and useful for device development benefit to shed light on the net charge change on the surface oxygen atoms and in each layer of the Ag after NH_3 adsorption. Combining charge analysis, we found that from the bottom Ag layer to the surface O layer (four Ag layers and one O layer in continual sequence), the net charge transfer is +0.0016 e, +0.0004 e, −0.0004 e, −0.0222 e, and +0.0244 e, respectively, indicating that the first two Ag layer lose charges while the other two Ag layers and O atoms obtain charges. Therefore, the net charge dramatically changes in the first Ag layer from the top and in the surface O layer, suggesting that the top AgO surface dominates the entire charge transfer.

For gas sensors, sensing response time is one of the most important properties. We have extracted the sensing response time of our sensor by defining the response time as the time needed for the sensor to change over 63.2% of the maximum sensitivity (corresponding to one time constant in a first-order dynamic system). An analysis of Figure 2c shows that the response time for the Ag NC−MWCNTs hybrid sensor is ~7 s. It is comparable with that of an Ag mesowire NH_3 sensor (~5 s) for gas concentrations above 1%.[18] It is also comparable with the ultrafast room-temperature NH_3 sensor made of reduced graphene oxide (RGO), which has a response time of ~10 s.[42] But the RGO sensor has to be gated with a positive voltage (e.g., +40 V). Otherwise, the response is on the order of minutes.[43,44] In contrast, the response time is ~344 s for the

bare MWCNTs sensor. So it is clear that Ag NCs dramatically improve the sensing response. MWCNTs have very high carrier mobility (>100,000 $cm^2/(V\ s)$),[45] and the electronic state of MWCNTs would change rapidly with the change of the Ag oxidation state (Otherwise, the response for any gas is slow). Therefore, the response time could be mainly determined by the charge transfer between the gas molecules and Ag NCs. The fast response of our sensor suggests that NH_3 can easily adsorb on an Ag surface with a fast charge transfer. This also can be evidenced by a relatively flat response plateau after the rapid increase period, indicating that NH_3 molecules on an Ag surface are saturated after a short time.

The sensor recovery process was carried out in dry air. From Figure 2c, it can be seen that the sensor can recover to the initial state within 5 min. We have analyzed other sensing cycles, and the average time for full recovery was about 7 min, which is much shorter than that (12 min) of the positively-gated RGO NH_3 sensor.[42] For an RGO without a positive gate, it will take hours or days to complete the full recovery.[43,44] Here, we defined the recovery time as the time needed for the sensor to recover over 63.2% of the maximum sensitivity. According to the data analysis for our sensor, the recovery times are ~15 s and ~410 s for the Ag NC−MWCNTs hybrid and bare MWCNTs, respectively. Generally, it takes a very long time (more than overnight with our experiments) for the CNTs to recover to its initial state at room temperature, which could be attributed to the high binding energy between NH_3 molecules and CNT defects and the adsorbed oxygen.[15,30] However, in the Ag NC−MWCNTs hybrid sensor, Ag NCs could occupy these sites and become the dominating sensing element. The fast recovery speed suggests that the desorption barrier on the Ag surface is low for NH_3 molecules, probably because of the low binding energy of 0.36 eV as predicted from our DFT calculation. To study the stability of the Ag NC−MWCNTs hybrid sensor, we performed five sensing cycles (as shown in Figure 2d) to 1% NH_3 at room temperature. The sensing behavior appears quite repeatable.

Figure 4a shows the dynamic response ($\Delta R/R$) of the Ag NC−MWCNTs hybrid sensor when exposed to different

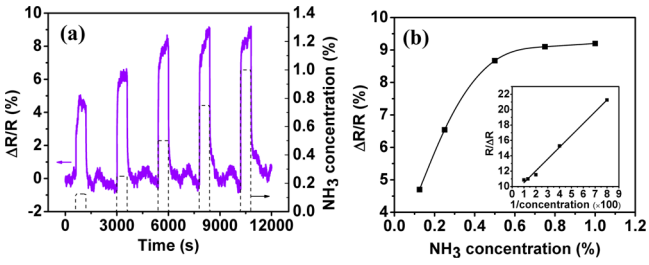

Figure 4. (a) Dynamic response ($\Delta R/R$) of the Ag NC−MWCNT hybrid sensor when exposed to different concentrations (C) of NH_3. (b) Curve fit of the sensor response ($\Delta R/R$) as a function of NH_3 concentration. The inset is a linear fitting of $1/S$ ($R/\Delta R$) vs $1/C$.

concentrations (C) of NH_3. The sensitivity increases monotonically from ~5 to 9% with increasing gas concentrations from 0.125 to 1%. Figure 4b plots the derived sensor response as a function of NH_3 concentrations. It can be seen that the sensor sensitivity increases rapidly when the gas concentration is relatively low. At higher gas concentrations, it becomes saturated probably because of lacking Ag surfaces for further gas adsorption. This curve can be well described by the following equation[4]

$$S = \frac{\alpha}{1 + \frac{\beta}{C}}$$

where α = 0.1115, which is a constant without units, and β = 1.7148×10^{-1}, which is a constant with the same units as concentration (%). The linear fitting of $1/S$ versus $1/C$ is shown in the inset of Figure 4b, which can be explained with the Langmuir isotherm.[4,46] When the concentration is in the lower region (about <0.4% in our case), the equation could be simplified as $S = (\alpha/\beta)C$, which suggests that the sensitivity and the concentration have a linear relationship. Meanwhile, high concentrations of ammonia tend to lead to a saturated response behavior.

Selectivity is also an important property of a gas sensor. To understand the selectivity of our sensor, we measured the sensing response of the same Ag NC−MWCNTs hybrid sensor to several other gases, including reducing gases such as H_2 and CO and an oxidizing gas such as NO_2. The sensing test cycle is the same as that for NH_3. Our results show that the Ag NC−MWCNTs hybrid sensor has excellent selectivity to NH_3 among all test gases. As shown in Figure 5, the sensor has

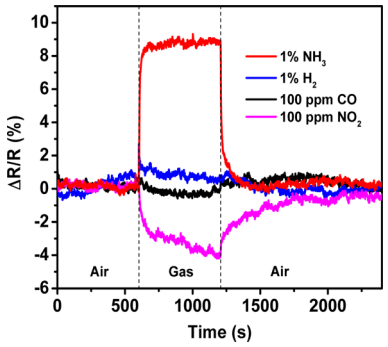

Figure 5. Comparison of sensing response to various gases.

negligible response to both 1% H_2 and 100 ppm CO. This result indicates that NH_3 is preferable for our Ag NC−MWCNTs hybrid sensor among common reducing gases, which act as electron donors. Nitrogen dioxide is an oxidization gas and an electron acceptor. The sensing response to 100 ppm NO_2 shows that the resistance of the Ag NC−MWCNT hybrid sensor decreases, suggesting a charge transfer from the hybrid to NO_2 molecules. The sensitivity gradually increased to an absolute value about 4% within 10 min exposure at room temperature.

The reliability of the Ag NC−MWCNTs hybrid sensor was studied by comparing its original sensing performance with its performance after 4 months of storage in air. As shown in Figure 6, the sensor still responded well toward NH_3 with slight degradation after four months, which indicates that the sensor is relatively stable in air. The same sensor after four-month storage was also tested against different concentrations of NH_3. The result (see Figure S5 in the Supporting Information) shows that the sensor can detect a concentration as low as 10 ppm, and the sensitivity gradually increased with increasing NH_3 concentrations ranging from 10 to 10 000 ppm (1%).

CONCLUSIONS

We have demonstrated fabrication and application of an Ag NC−MWCNTs hybrid structure for room-temperature NH_3 gas sensors. The as-produced Ag NC−MWCNTs hybrid sensor

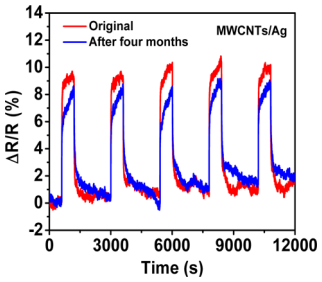

Figure 6. Comparison of sensing performance toward 1% NH_3 before and after 4 months of storage in air.

showed much higher sensitivity than CNTs alone. Fast sensing response and recovery were also achieved by the deposition of Ag NCs on MWCNTs. The Ag NCs work as the dominant active sites for NH_3 adsorption in the sensing process. A net charge transfer from NH_3 to Ag quickly occurs after adsorption. At low concentrations of NH_3, there is a linear relationship between the sensitivity and the concentration. The hybrid sensor has an excellent selectivity to NH_3 because it prefers to respond to NH_3 instead of other reducing gases such as H_2 and CO. Our DFT calculation reveals that the NH_3 molecules prefer to adsorb above the Ag hollow sites that are not occupied by oxygen atoms on AgO surface with H pointing toward Ag. The hybrid sensor also shows a good stability in air. Therefore, the Ag NC−MWCNT hybrid is attractive for selective detection of NH_3 at room temperature. The sensor fabrication process is simple and low cost, thereby promising for large-scale applications.

■ ASSOCIATED CONTENT

Ⓢ Supporting Information

Additional figures. This material is available free of charge via the Internet at http://pubs.acs.org.

■ AUTHOR INFORMATION

Corresponding Author

*E-mail: jhchen@uwm.edu.

Notes

The authors declare no competing financial interest.

■ ACKNOWLEDGMENTS

The authors acknowledge financial support from the National Science Foundation (CMMI-0856753 and ECCS-1001039), and from the Research Growth Initiative Program of the University of Wisconsin Milwaukee (UWM). The SEM imaging was conducted at the UWM Bioscience Electron Microscope Facility, and TEM analyses were conducted in the UWM Physics HRTEM Laboratory. Sensor electrodes were fabricated at CNM of Argonne National Laboratory, supported by U.S. DOE (DE-AC02-06CH11357).

■ REFERENCES

(1) Collins, P. G.; Bradley, K.; Ishigami, M.; Zettl, A. *Science* **2000**, *287*, 1801−1804.
(2) Du, N.; Zhang, H.; Chen, B. D.; Ma, X. Y.; Liu, Z. H.; Wu, J. B.; Yang, D. R. *Adv. Mater.* **2007**, *19*, 1641−1645.
(3) Lu, G. H.; Ocola, L. E.; Chen, J. H. *Adv. Mater.* **2009**, *21*, 2487−2491.
(4) Zhang, D. H.; Liu, Z. Q.; Li, C.; Tang, T.; Liu, X. L.; Han, S.; Lei, B.; Zhou, C. W. *Nano Lett.* **2004**, *4*, 1919−1924.
(5) Iijima, S. *Nature* **1991**, *354*, 56−58.
(6) Dalton, A. B.; Collins, S.; Munoz, E.; Razal, J. M.; Ebron, V. H.; Ferraris, J. P.; Coleman, J. N.; Kim, B. G.; Baughman, R. H. *Nature* **2003**, *423*, 703−703.
(7) Deheer, W. A.; Chatelain, A.; Ugarte, D. *Science* **1995**, *270*, 1179−1180.
(8) Javey, A.; Guo, J.; Wang, Q.; Lundstrom, M.; Dai, H. J. *Nature* **2003**, *424*, 654−657.
(9) Li, J.; Lu, Y. J.; Ye, Q.; Cinke, M.; Han, J.; Meyyappan, M. *Nano Lett.* **2003**, *3*, 929−933.
(10) Kong, J.; Franklin, N. R.; Zhou, C. W.; Chapline, M. G.; Peng, S.; Cho, K. J.; Dai, H. J. *Science* **2000**, *287*, 622−625.
(11) Zhao, J. J.; Buldum, A.; Han, J.; Lu, J. P. *Nanotechnology* **2002**, *13*, 195−200.
(12) Li, Y. H.; Zhao, Y. M.; Zhu, Y. Q.; Rodriguez, J.; Morante, J. R.; Mendoza, E.; Poa, C. H. P.; Silva, S. R. P. *Carbon* **2006**, *44*, 1821−1825.
(13) Penza, M.; Cassano, G.; Rossi, R.; Alvisi, M.; Rizzo, A.; Signore, M. A.; Dikonimos, T.; Serra, E.; Giorgi, R. *Appl. Phys. Lett.* **2007**, *90*, 173123.
(14) Kong, J.; Chapline, M. G.; Dai, H. J. *Adv. Mater.* **2001**, *13*, 1384−1386.
(15) Robinson, J. A.; Snow, E. S.; Badescu, S. C.; Reinecke, T. L.; Perkins, F. K. *Nano Lett.* **2006**, *6*, 1747−1751.
(16) Mubeen, S.; Zhang, T.; Yoo, B.; Deshusses, M. A.; Myung, N. V. *J. Phys. Chem. C* **2007**, *111*, 6321−6327.
(17) Brahim, S.; Colbern, S.; Gump, R.; Grigorian, L. *J. Appl. Phys.* **2008**, *104*, 024502.
(18) Murray, B. J.; Walter, E. C.; Penner, R. M. *Nano Lett.* **2004**, *4*, 665−670.
(19) Timmer, B.; Olthuis, W.; van den Berg, A. *Sens. Actuators, B* **2005**, *107*, 666−677.
(20) van der Eerden, L. J. M.; de Visser, P. H. B.; van Dijk, C. J. *Environ. Pollut.* **1998**, *102*, 49−53.
(21) Mao, S.; Cui, S. M.; Yu, K. H.; Wen, Z. H.; Lu, G. H.; Chen, J. H. *Nanoscale* **2012**, *4*, 1275−1279.
(22) Cui, S. M.; Lu, G. H.; Mao, S.; Yu, K. H.; Chen, J. H. *Chem. Phys. Lett.* **2010**, *485*, 64−68.
(23) Cui, S. M.; Mattson, E. C.; Lu, G. H.; Hirschmugl, C.; Gajdardziska-Josifovska, M.; Chen, J. H. *J. Nanopart. Res.* **2012**, *14*, 1−13.
(24) Weinert, M.; Schneider, G.; Podloucky, R.; Redinger, J. *J. Phys.−Condens. Mater.* **2009**, *21*, 084201.
(25) Perdew, J. P.; Burke, K.; Ernzerhof, M. *Phys. Rev. Lett.* **1996**, *77*, 3865−3868.
(26) Hirshfeld, F. L. *Theor. Chim. Acta* **1977**, *44*, 129−133.
(27) Odom, T. W.; Huang, J. L.; Kim, P.; Lieber, C. M. *Nature* **1998**, *391*, 62−64.
(28) Chen, J. H.; Lu, G. H.; Zhu, L. Y.; Flagan, R. C. *J. Nanopart. Res.* **2007**, *9*, 203−213.
(29) Bachtold, A.; Strunk, C.; Salvetat, J. P.; Bonard, J. M.; Forro, L.; Nussbaumer, T.; Schonenberger, C. *Nature* **1999**, *397*, 673−675.
(30) Peng, N.; Zhang, Q.; Chow, C. L.; Tan, O. K.; Marzari, N. *Nano Lett.* **2009**, *9*, 1626−1630.
(31) Batzill, M.; Diebold, U. *Prog. Surf. Sci.* **2005**, *79*, 47−154.
(32) Raju, N. R. C.; Kumar, K. J.; Subrahmanyam, A. *J. Phys. D: Appl. Phys.* **2009**, *42*, 135411.
(33) Giovannetti, G.; Khomyakov, P. A.; Brocks, G.; Karpan, V. M.; van den Brink, J.; Kelly, P. J. *Phys. Rev. Lett.* **2008**, *101*, 026803.
(34) Kosynkin, D. V.; Higginbotham, A. L.; Sinitskii, A.; Lomeda, J. R.; Dimiev, A.; Price, B. K.; Tour, J. M. *Nature* **2009**, *458*, 872−876.
(35) Li, X. L.; Wang, X. R.; Zhang, L.; Lee, S. W.; Dai, H. J. *Science* **2008**, *319*, 1229−1232.
(36) Law, J. B. K.; Thong, J. T. L. *Nanotechnology* **2008**, *19*, 205502.
(37) Du, N.; Zhang, H.; Chen, B. D.; Ma, X. Y.; Liu, Z. H.; Wu, J. B.; Yang, D. R. *Adv. Mater.* **2007**, *19*, 1641−1645.
(38) Bartolucci, F.; Franchy, R.; Barnard, J. C.; Palmer, R. E. *Phys. Rev. Lett.* **1998**, *80*, 5224−5227.
(39) Petrov, V. V.; Nazarova, T. N.; Korolev, A.; Kopilova, N. F. *Sens. Actuators, B* **2008**, *133*, 291−295.

(40) Bultinck, P.; Van Alsenoy, C.; Ayers, P. W.; Carbo-Dorca, R. *J. Chem. Phys.* **2007**, *126*, 144111.
(41) Yamazoe, N. *Sens. Actuators, B* **1991**, *5*, 7−19.
(42) Lu, G. H.; Yu, K. H.; Ocola, L. E.; Chen, J. H. *Chem. Commun.* **2011**, *47*, 7761−7763.
(43) Schedin, F.; Geim, A. K.; Morozov, S. V.; Hill, E. W.; Blake, P.; Katsnelson, M. I.; Novoselov, K. S. *Nat. Mater.* **2007**, *6*, 652−655.
(44) Lu, G. H.; Park, S.; Yu, K. H.; Ruoff, R. S.; Ocola, L. E.; Rosenmann, D.; Chen, J. H. *ACS Nano* **2011**, *5*, 1154−1164.
(45) Durkop, T.; Getty, S. A.; Cobas, E.; Fuhrer, M. S. *Nano Lett.* **2004**, *4*, 35−39.
(46) Del Bubba, M.; Arias, C. A.; Brix, H. *Water Res.* **2003**, *37*, 3390−3400.